Ceramic enamels as new back contacts for Cu(In,Ga)Se_2 based photovoltaic tile

Diego Fraga*, Teodora Stoyanova Lyubenova, Aitor Rey, Ivan Calvet, Rafael Martí, Juan B. Carda

Department of Organic and Inorganic Chemistry, Jaume I University, Av. de Vicent Sos Baynat s/n, 12071, Castellón (Spain)

Abstract

In this work, we investigated the properties of silver and gold enamels as potential back contacts for Cu(In,Ga)Se_2 (CIGS) solar cells. The enamels were deposited on ceramic tiles by non-vacuum printing techniques. Thus, we are proposing a development of integrated photovoltaic tile for the first time. We also explained the CIGS synthesis procedure using co-precipitation of selenites precursors. To deposit the precursor powders on the substrate, a doctor blade method is applied. The interface morphology between ceramic tile, back contact, and CIGS absorber was studied as a critical factor for the final solar cell performance. The thermal treatment effect on the back contact properties was also reported.

Excellent compatibility between CIGS and gold layer was observed, keeping thickness and chemical composition adequate for photovoltaic applications. The band gap energy confirms assembly effectiveness. Unsatisfied results of silver diffusion towards CIGS absorber were obtained when silver enamels were used.

* Corresponding author: tel.: +34 964 728234; fax: +34 964 729016

E-mail address: fraga@uji.es (D. Fraga)

1. Introduction

Thin film technology is a desired alternative for preparing photovoltaic devices because of an enormous saving of costly materials and simplification of the manufacturing process. The low-cost potential of this technology is rooted by means of cheaper substrate applications, effective uses of raw materials and thinner coatings (ranging from 1.5 to 3 μm) [1, 2]. In this sense, ceramic tiles emerge as good alternatives for substrate by reducing production costs and giving benefits to the final products. An advantage is a possibility to use higher temperature treatments, keeping intact material thermal stability. The photovoltaic (PV) incorporation in building constructions as an energy source by replacing of conventional building materials (as roof, skylights, or facades) makes them very attractive for so called Building Integrated Photovoltaics (BIPV) [3, 4]. In addition, these systems can provide large areas of photovoltaic modules based on diverse absorbers.

$Cu(In,Ga)Se_2$ (CIGS) is an attractive absorber for thin film solar cells due to its unique optical and electrical properties [5-7]. CIGS technology has recorded 21.7% of efficiencies[8]. The typical CIGS solar cell is constituted for soda-lime glass substrate (3 mm), sputtered molybdenum back contact (800 nm), CIGS absorber layer (2 μm), chemical bath deposited CdS buffer layer (10-60 nm), sputtered zinc oxide (i:ZnO) or/and indium tin oxide (ITO) as window layer [9]. The use of vacuum-based technique for thin film deposition is a main handicap of this technology[10, 11]. Covering at room temperature and atmospheric pressures stand out as an attractive alternative for the absorber layers[12-17]. Methods as doctor blade, spin coating, and dip-coating are very suitable for that purpose, being cost-effective ways of preparation. In this connection, the doctor blade technique is very desirable from an industrial point of view for large-scale production due to its simplicity and availability at many factories (e.g ceramic tile

industrial units)[10, 18]. The doctor blade, also known as tape casting, is a processing method for producing of thin films on large area surfaces with no waste of materials and good layer uniformity. Commonly, this method involves spreading through a moving blade onto a stationary substrate. There are three different type of doctor blade coating devices in use: a knife, a rectangular frame and a spiral film applicator[19]. The gap size of the blade governs the layer thickness. The micrometric precision of blade regulation is the main inconvenient of this way of deposition that leads difficult precise depth control. However, controlling coating parameters that influence to the film formation as surface energy of the substrate, surface tension of the fluid, coating or blade speed, fluid viscosity, density, and surface temperatures could solve this problem [20, 21].

The soda-lime glass is probably the most used substrate in CIGS solar cell [22]. Polymers and metals are also investigated as alternative options [23-26]. Polymers have appropriate chemical inertness and do not react with selenium during the thermal treatment [23]. In addition, these materials have a smoother surface and humidity barrier. However, they have low thermal stability to withstand thermal selenization treatment.

In contrast, metals have better thermal stability than polymers, but a barrier layer is required to block impurities that can diffuse toward the absorber layer. Concerning these drawbacks, the ceramics are good alternative substrates. The principal selection criteria that ceramics must fulfill are: compatible thermal expansion coefficient (CTE) (~ $7 \cdot 10^{-6}$ K^{-1}), excellent thermal (T > 600 ºC) and chemical resistivity and being suitable for industrial uses in terms of costs and facilities. The CTE of ceramics is similar to the CTE of CIGS (8-11$\cdot 10^{-6}$ K^{-1}) [23] and is relatively cheap product. Thus, ceramic tiles for substrates offer new possibilities for solar cells and its integration in urban areas (BIPV).

Commonly, the back contact layer is made of metal. It fabrication is well studied part of materials engineering field. The main requirements for a good back contact for CIGS solar cells are: inertness, smooth surface, good electrical properties (low contact resistance), good thermal stability and cost, and it should act as diffusion barrier. The surface morphology plays a key role in the final electrical properties. The back contact executed as a barrier acts as impurities diffusion membrane between the substrate and the absorber [23]. Variety of metal/ CIGS contacts have been investigated, including (Cu, Ni, Al, Mo, Pt)[27-29], Ag[30], Au[31] and others (W, Cr, Ta, Nb, V, Ti, Mn)[32, 33] with limited success. The most applied metal is molybdenum (Mo). Despite of that, Mo deposition also presents certain problems related to bad substrate adhesion and fast metal oxidation[33-36]. The back contacts used for high- efficiency devices, is typically deposited by direct current (dc) sputtering [37, 38], evaporation [39, 40] or chemical vapour deposition (CVD) [41] that increase the final value of the cell.

Although CIGS semiconductor has been studied for several decades, rather limited information has been reported in literature on metal morphology effects on the back contact resistance.

The paper reports a development of new back contacts for CIGS solar cells. Substrate made by common porcelain stoneware ceramic tile is used. The tile was previously covered with industrial glazes containing gold or silver in its compositions. The glaze, situated between the CIGS absorber and the substrate, provides chemical stability, inertness and roughness reduction. The glass nature of the enamels simulates flat surface with no porosity. The metal (gold or silver) content allows it to operate as a metal back contact. Non-vacuum, solution-based, and large-scale way of deposition, called ink printing, of the enamels for reducing materials and costs is suggested. In addition, simple way of preparation using co-precipitation route for the CIGS absorber

is also reported. The developed powders were deposited on the substrate by doctor blade technique. The morphological properties in the interface ceramic tile/ back contact/CIGS were investigated as crucial aspect for the final solar cell performance. Band gap energy was measured for the optimal sample testing the assembly effectiveness.

2. Experimental details

2.1 Support preparation

Porcelain stoneware substrates (5 mm thickness) were made by industrial method of preparation using kaolinitic clay, feldspar and feldspathic sand. The pastes (with average chemical composition (oxide weights %): 60-70 SiO_2, 18-20Al_2O_3, 1.5-3 K_2O, 3.5- 4.5 Na_2O, 1-2 others oxides, were prepared by pressing and further sintering in a conventional kiln.

Industrial frit developed for the enamel applied in the solar cell contains the following average composition (oxide weights %): 55-65 SiO_2, 10-30 Al_2O3, 0.5-5 Na_2O-K_2O, 13 -17 MgO-CaO, 10-20 others. The frits were applied in order to ensure low porosity, impermeability and to provide chemical stability and roughness reduction simulating thereby glass surface.

The gold dye over the frit was deposited by ink-jet printing in non-vacuum conditions for obtaining gold conductive enamel with a thickness ~ 200 nm. The same procedure was applied for the silver enamel (~ 2.50 µm thickness), but the silver dye was deposited by screen printing technique. These coating methodology, ink-jet and screen-printing, were selected to determine their effectiveness. They achieved different layer depths and morphologies that may influence to the device properties. On Figure 1 schematic design of the photovoltaic ceramic tile is shown.

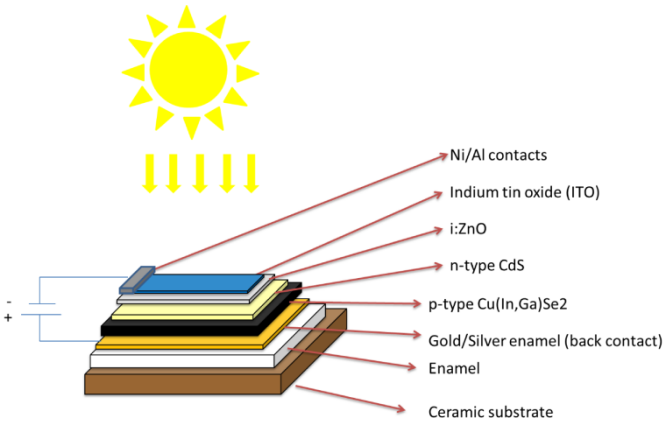

Figure 1. Schematic layout of a Cu(InGa)Se_2-based photovoltaic ceramic tile.

2.2 CIGS synthesis and deposition

$CuIn_{0.7}Ga_{0.3}Se_2$ solid solution was synthesized using co-precipitation route of metal selenite precursors, keeping atomic ratio of Cu/(In + Ga) = 0.92 and Ga/(In+Ga) = 0.3 [1, 42]. The resulting CIGS powder was further mixed with triethanolamine (TEA, 99%, Riedel-de Haën) and ethanol (C_2H_5OH, 99.9%, Sharlau) to form slurry that was deposited on ceramic substrate by manual knife doctor blade method. The slurry viscosity and the blade gap mainly govern the thickness precision.

The obtained layer was pre-heated on a hot plate at 400ºC for 2 min to remove partially the solvent and to encourage further precursor decomposition. Finally, the CIGS films were selenized under reducing atmosphere (5% H_2/ 95% N_2) in a tubular furnace. The applied thermal cycle corresponds to heating velocity rate of 20 ºC/min up to maximum temperature of: 200 °C (sample A); 350 ºC (sample B); 450 ºC (sample C); 500 ºC (sample D) and 550 ºC (sample E). Free cooling and no soaking time were applied.

2.3 Characterization techniques

Crystal structure of powders and films was monitored by X-ray diffraction (XRD) using a D4 Endeavor, Bruker-AXS equipped with a Cu Kα radiation source. Data were

collected by step-scanning from 10º to 80º with step size of 0.05º 2θ and 1 s counting time per step.

The particle sizes were quantitatively evaluated from the XRD data using the Debye-Scherrer equation[43],

$$D = \frac{k\lambda}{\beta \cos\theta} \quad (1)$$

where k is Scherrer constant (0.89), λ the X-ray wavelength (0.15405 nm), β the peak width of half-maximum, and θ is the Bragg diffraction angle.

Scanning Electron Microscopy (SEM) model JEOL 7001F attached with an energy dispersive X-ray analysis (EDX) was employed to study the morphology and elemental composition of the films. The layer thickness was determined from cross section micrographs. The glaze surfaces were studied by Atomic Force Microscope (AFM) with a JSPM-5200 JEOL Scanning Probe Microscope operating in contact approach. Adhesion between back contact layers and support was measured using laboratory test method by applying and removing tape and scratching of the surface. This method is used to establish whether the adhesion of a coating to a substrate is at a generally adequate level. The films electrical resistance was measured using a digital multimeter (Volt-Ohm meter).

Optical properties and band gap energy of the CIGS layer was conducted by UV–Vis-NIR spectroscopy in the wavelength range 200-1200 nm (step size 1 nm) using Cary 500 Scan Varian spectrophotometer. The absorption spectra were obtained applying $BaSO_4$ integrating sphere as a white reference material.

3. Results and Discussion

3.1 Ceramic substrate

Physical characteristics of the ceramic body were analyzed. The obtained tiles density was 2.056 g/cm^3 after thermal treatment at 1200 °C (data not shown). The vitrification plot displayed linear contraction of 7.56 % and water absorption of 0.98 % at 1165 ºC. These values remained constant even at 1190 °C, where the water absorption decreases up to 0 % (data not shown).

3.2 Gold enamel

Figure 2(a) displays AFM images of the Au enamel layer. Rather smooth and regular surface of polycrystalline gold enamel is observed. The average roughness is about 3 nm, very suitable for layer applications. There are some isolated grains disperse on the surface, but this fact does not harm layer functionality. The gold cover is dense and well-adhered to the ceramic substrate (Fig. 2b). The estimated, from the cross-section micrograph, layer thickness is ~ 200 nm (Fig. 2b). Homogeneous grain distribution of particles with 50 nm average dimensions (Fig. 2c) suggests excellent coating properties.

Figure 3 displays the X-ray diffraction pattern of Au layer before CIGS deposition. The sample reveals various diffraction peaks related to SiO_2 (quartz, JCPDS card, file No 01-083-2471) at 27.1º (2θ) and SiO_2 (cristobalite, JCPDS card, file No 01-076-0939) at 21.8º and 35.8º (2θ). The reflections indexed with (1,1,1), (2,0,0), (2,2,0) and (3,1,1) belong to Au (JCPDS card, file No 01-1172). The SiO_2 compounds in the pattern are coming from the glaze layer below. This demonstrates that the Au layer is very thin that may affect to the device properties.

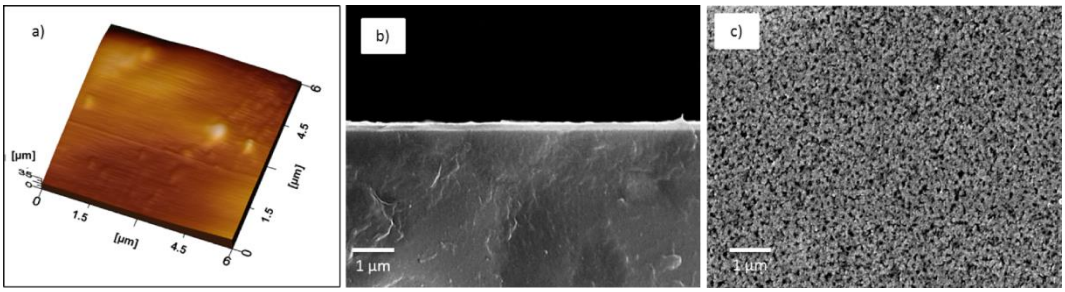

Figure 2. Surface morphology of Au thin film: a) AFM surface image; b) SEM cross-section micrograph of Au layer and c) SEM micrograph of Au surface.

The Au particle sizes were quantitatively evaluated from the XRD data (Fig. 3) using the Debye-Scherrer equation (1). From the (1,1,1), (2,0,0) and (2,2,0) d-spacing's crystallite dimensions were calculated. The particles measure from 20 nm to 50 nm. The result fits well with the microscope observations (Fig. 2c).

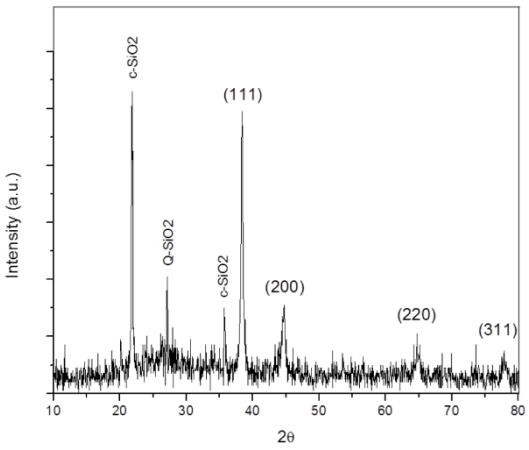

Figure 3. X-ray diffraction pattern of Au layer before CIGS deposition.

X-ray diffractograms of samples A, B, C, D and E after CIGS thermal treatment are shown in Figure 4. The main diffraction peaks could be assigned to $CuIn_{0,7}Ga_{0,3}Se_2$ crystalline phase (JCPDS card, file No 35-1102). It can be notice that reflection intensities increase with temperature changes from 200º to 550 ºC. Additional peaks at

203 2θ = 38.3, 64.9, 44.6 and 77º are also found. These reflections could be associated to Au
204 (JCPDS card, file No 01-1172). Diffraction peaks at 2θ = 21.8, 30.8 and 35.7º
205 corresponds to SiO_2 (JCDPS card, file No 76-0939) and are coming from the glaze. No
206 secondary phases during the CIGS formation are detected.
207

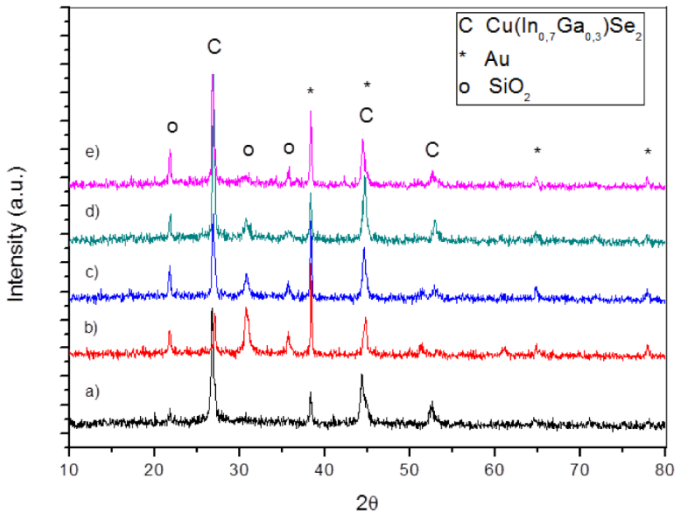

208

209 **Figure 4**. XRD of CIGS films after thermal treatment at: a) 200 ºC, b) 350 ºC, c) 450
210 ºC, d) 500 ºC and e) 550 ºC.
211

212 Figure 5 shows surface SEM images of CIGS films selenized at different temperatures.
213 The film crystallinity rise with temperature according to XRD results (Fig. 4). Surface
214 (Fig. 5a and 5b) and cross-section view (Fig. 6a and 6b) of the films obtained at low
215 temperatures shows cracks and pinholes. This result suggests unstuck to the substrate
216 coating. In order to improve the layer, higher temperatures were applied. After
217 treatment, the samples (Fig. 5c, 5d and 5e) show granular surface morphology that
218 decreases with sintering procedure. Finally, well-sintered dense coating with some
219 surface crystals at 500ºC (Fig. 5d) is detected. The gold layer thickness decrease from
220 300 nm (for sample heated at 200ºC) to 160 nm (for sample at 550ºC) due to precursor's
221 decomposition during calcination (Fig. 6). The sample calcined at 500ºC displays lack

222 of surface defects, good adhesion to the ceramic substrate and dense and microstructure.
223 As a result, it was selected among other samples as optimum.
224

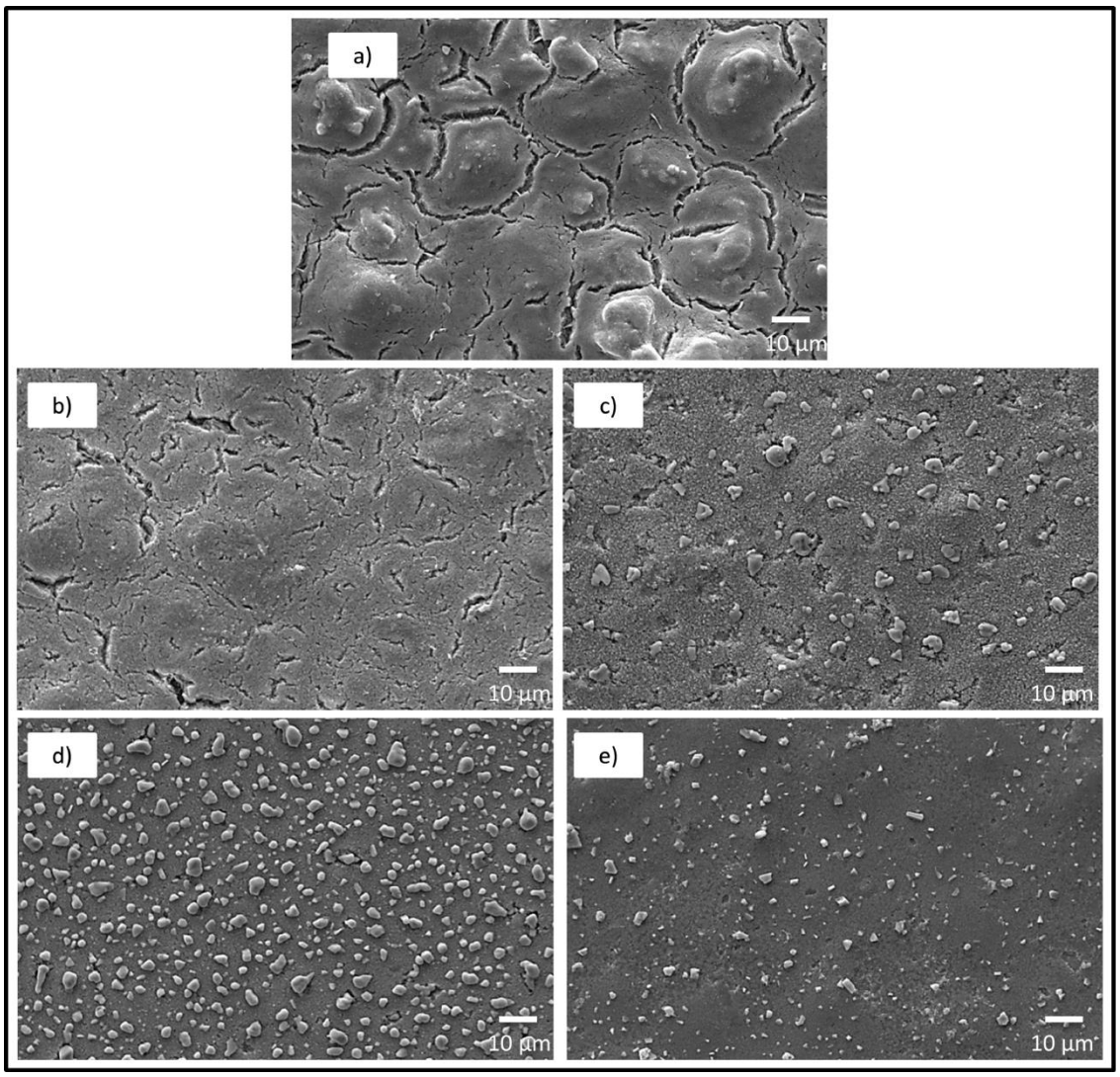

225

226 **Figure 5.** Surface micrographs of samples treated at: a) 200 ºC, b) 350 ºC, c) 450 ºC, d)
227 500 ºC and e) 550 ºC.
228
229 The film elemental composition was determined by energy-dispersive X-ray analysis
230 (EDX). Dotted lines in Figure 6 indicate the semi-quantitative analysis (atomic %) of
231 CIGS stoichiometry. The elemental concentration is indicated with dotes along the
232 depth in three different areas: bottom (1), middle (2) and top (3). The results in Table 1

prove a slight Au diffusion towards the CIGS absorber for samples (b), (c), (d) and (e). When temperatures up the Au diffusion increase and layer thickness decrease (Fig. 6 a-e). Nevertheless, the Au diffusion does not have an influence on the optical properties of the CIGS absorber and on the electrical resistance of the back contact. The Au layer still had electrical conductivity that was checked by Multimeter. The optical response is discussed hereafter.

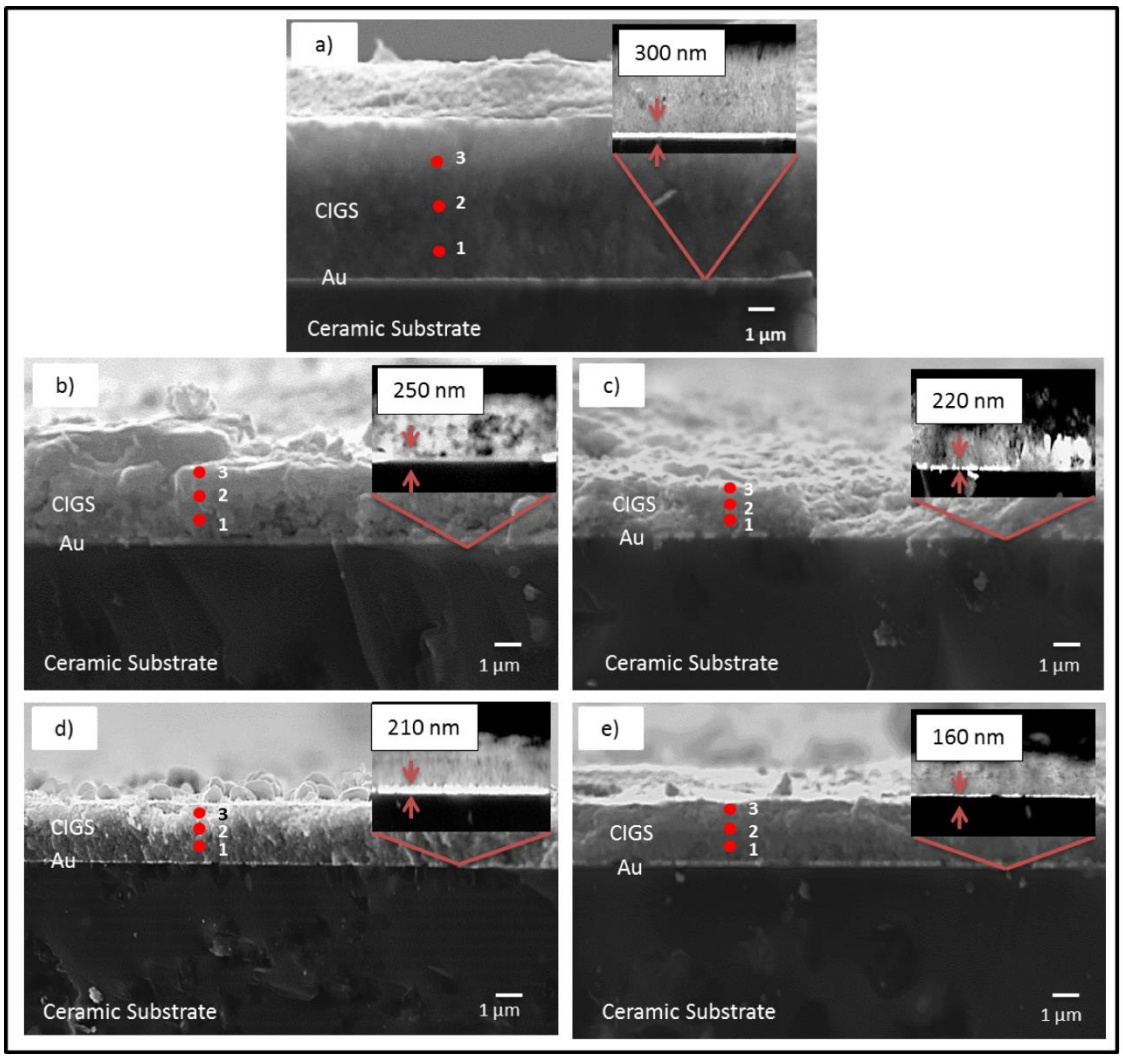

Figure 6. Cross-sections micrographs of samples treated at: a) 200 ºC, b) 350 ºC, c) 450 ºC, d) 500 ºC and e) 550 ºC.

The CIGS sample heated at 500ºC presents homogeneous chemical composition (Table 1 sample d). The extra Cu amount is according to the initial stoichiometry. At lower temperatures (samples a, b and c) selenium losses are detected. Unexpected more heterogeneous composition for sample (e) is observed despite of the applied higher temperature.

Table 1. EDX analysis (at %) and metal ratio of sample treated at: a) 200 ºC, b) 350 ºC, c) 450 ºC, d) 500 ºC and e) 550 ºC.

Sample	Point of analysis	Cu	In	Ga	Se	Au	Cu/In+Ga	Ga/In+Ga
a)	1	29.82	19.85	7.60	42.73	-	1.08	0.27
	2	28.40	19.76	8.17	43.67	-	1.01	0.29
	3	29.67	19.66	8.95	41.72	-	1.03	0.31
b)	1	22.95	49.06	11.68	15.38	0.93	0.37	0.19
	2	15.06	62.98	13.88	8.08	-	0.19	0.18
	3	13.05	65.82	12.63	8.50	-	0.16	0.16
c)	1	30.63	31.87	12.44	21.04	4.02	0.69	0.28
	2	41.78	19.53	6.60	30.08	2.01	1.59	0.25
	3	32.86	22.72	8.23	34.95	1.24	1.06	0.26
d)	1	22.45	17.51	5.27	51.42	3.35	0.98	0.23
	2	24.48	16.70	5.78	52.05	0.99	1.08	0.26
	3	25.86	17.46	6.31	49.44	0.93	1.08	0.27
e)	1	34.43	19.68	3.89	35.23	6.77	1.46	0.16
	2	33.48	21.07	4.51	37.03	3.91	1.30	0.17
	3	24.71	21.10	15.51	37.49	1.19	0.67	0.42

Band gap energy was measured only for sample “d” selected as optimum. Figure 7 shows band gap of approximately 1.18 eV that fits with the value corresponding to $Cu(In_{1-x}Ga_x)Se_2$ solid solution [44]. The result indicates that the detected gold diffusion does not concern the optical properties of the final device.

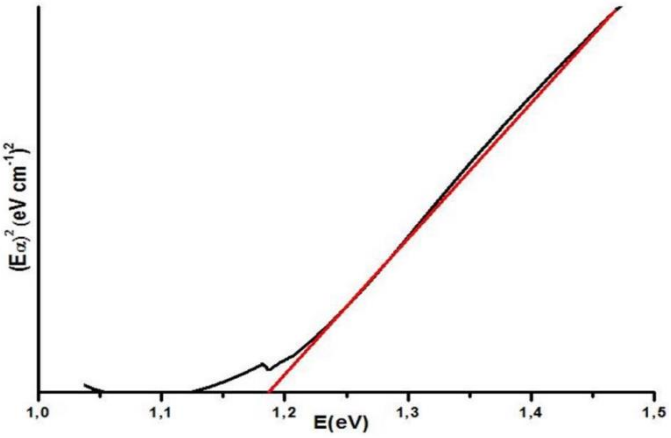

Figure 7. Plot of $(\alpha h\nu)^2$ as function of energy for CIGS sample "d".

3.2.1 Silver enamel

Figure 8 (a) display AFM images of the Ag glazed layer. Polycrystalline silver glaze with heterogeneous and roughness surface is observed. The average roughness is about 14 nm, suitable for layer applications. However, different embedded grains on the surface are detected.

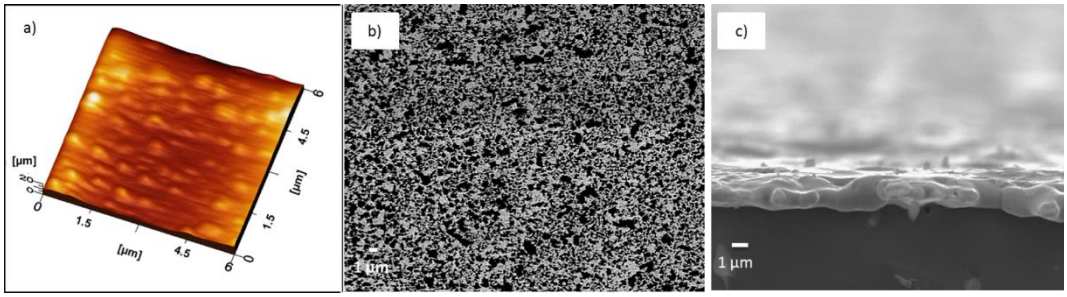

Figure 8. Surface morphology of Ag thin film: a) AFM surface image; b) SEM micrograph of Ag surface and c) SEM micrograph of cross-section of Ag layer.

Well-adhered to the ceramic substrate silver layer is assumed from Figure 8b and 8c. Layer thickness $\geq$ 2 µm is deduced from the cross-section image in Figure 8c. Heterogeneous grain distribution with sizes from 3nm to 500 nm is detected. To

confirm the particle dimensions, X-ray diffraction of the Ag layer before CIGS deposition was done (Fig. 9). The calculation using equation (1) of (1,1,1), (2,0,0) and (2,2,0) exposes crystal sizes corresponding to 176 nm, 88 nm and 196 nm that are agreed with the range (3-500 nm) discussed before.

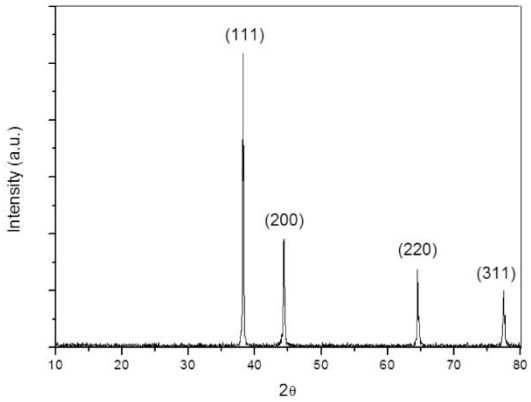

Figure 9. XRD pattern of Ag layer before CIGS deposition.

X-ray diffraction spectra of CIGS films treated at different condition are exposed in Figure 10. It can be emphasized that CIGS compound crystalizes even at 350ºC (Fig. 10b). The main reflections could be assigned to the $CuIn_{0,7}Ga_{0,3}Se_2$ (JCPDS card, file No 35-1102). Peaks intensities increase with temperature (Fig. 10b-e). Reflections at 2θ = 38.2, 44.4, 64.6 and 77.5º are related to Ag (JCPDS card, file No 01-087-0718). Secondary phase of Ag_2Se compound (2θ = 30.99, 32.78, 33.56, 34.82, 37.04 and 42.73º) (JCPDS card, file No 00-020-1063) is also distinguished. This result concludes that Ag diffuse towards the absorber layer (Table 2). Diffraction peaks at 2θ = 21.8, 30.8 and 35.7º is assigned to SiO_2 (JCPDS card, file No 76-0939).

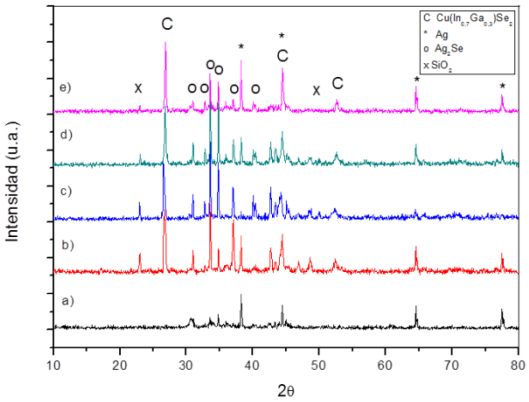

Figure 10. XRD of films treated at temperatures: a) 200 ºC, b) 350 ºC, c) 450 ºC, d) 500 ºC and e) 550 ºC.

SEM surface images of CIGS films treated at different temperatures are exposed in Figure 11. Granular surface morphology and increasing with temperature grains can be observed. Sintering processes at higher temperatures are deduced (Fig. 11 c and d). The cross-section micrographs on Figure 12 show unstuck to the substrate coatings for all temperatures. This result could be ascribed to the way of deposition (e.g screen printing). Holes and irregular morphology for all samples is remarked. The layer´s elemental composition (Table 2) confirms silver diffusion and heterogeneities. The silver enamel is unstable under thermal treatment. The layer results non-ohmic. Any further characterizations for the Ag system were avoided.

306 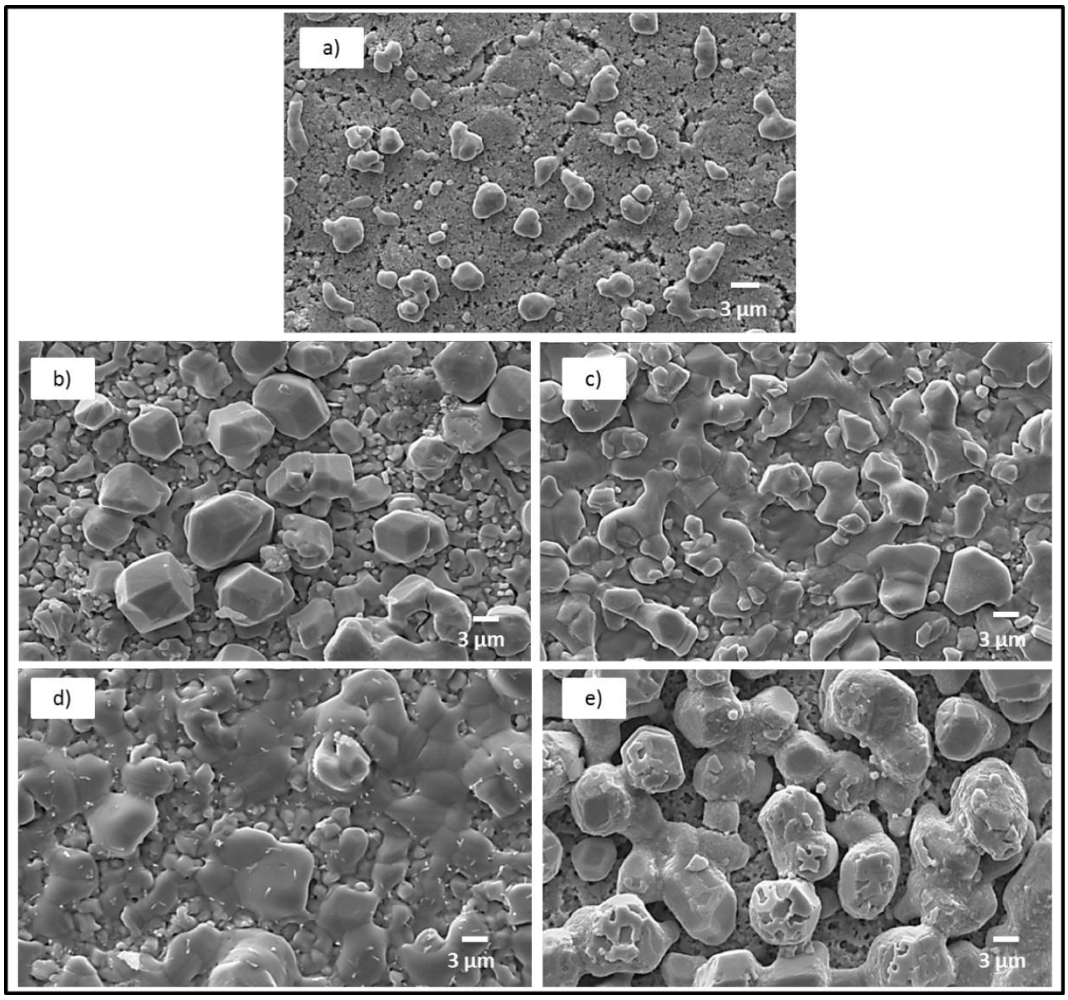

307 **Figure 11.** SEM surface images of samples heated at: a) 200 ºC, b) 350 ºC, c) 450 ºC, d)

308 500 ºC and e) 550 ºC.

309

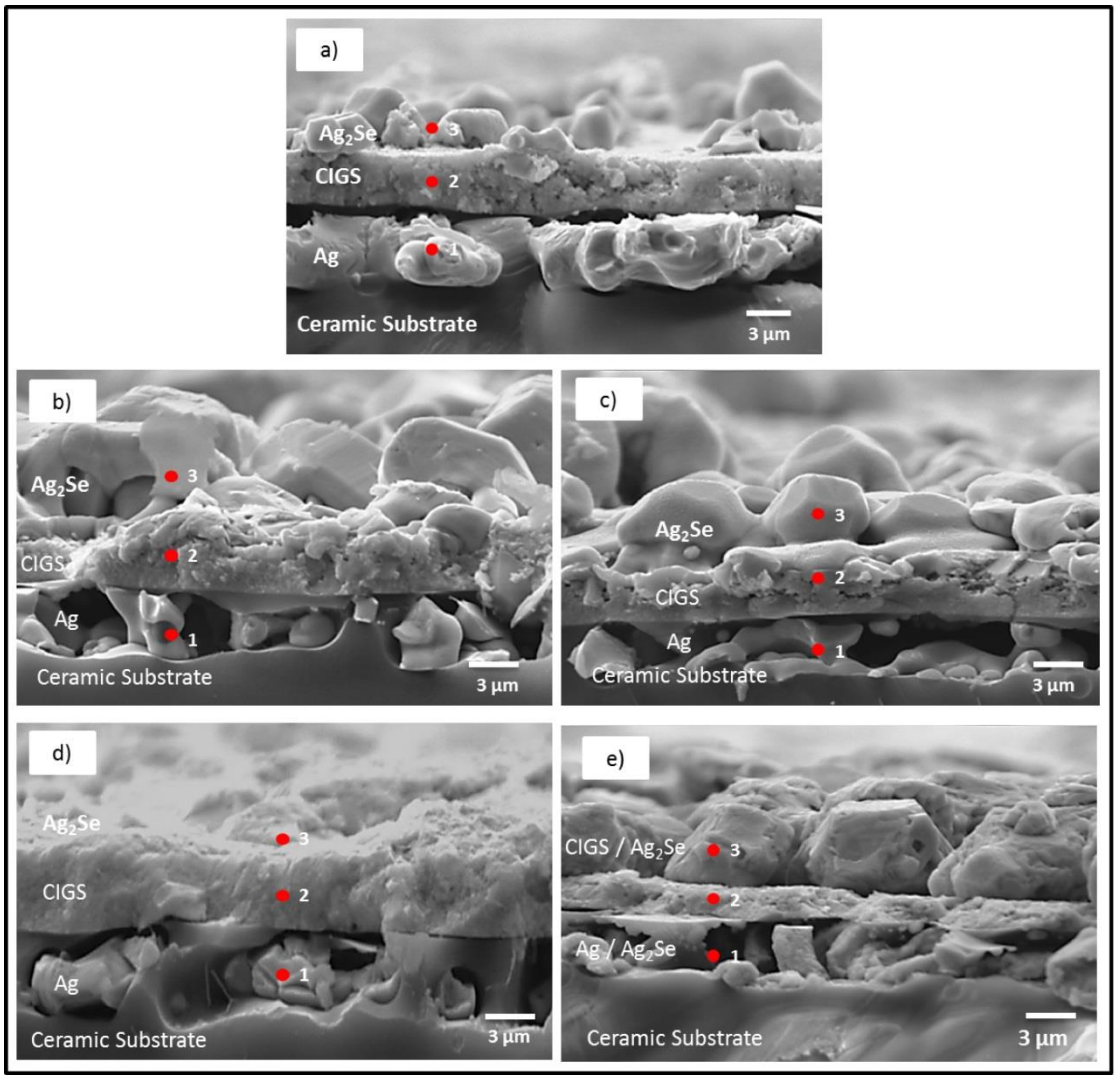

Figure 12. SEM cross-section images of samples heated at: a) 200 ºC, b) 350 ºC, c) 450 ºC, d) 500 ºC and e) 550 ºC.

Table 2. EDX analysis (atomic %) and metal ratio of sample heated at: a) 200 ºC, b) 350 ºC, c) 450 ºC, d) 500 ºC and e) 550 ºC.

Sample	Point of analysis	Cu (at%)	In (at%)	Ga (at%)	Se (at%)	Ag (at%)	Cu/In+Ga	Ga/In+Ga
a)	1	-	-	-	-	100	-	-
	2	20.25	10.87	4.49	17.03	47.36	1.32	0.29
	3	-	-	-	27.31	72.69	-	-
b)	1	-	-	-	30.22	69.78	-	-
	2	22.49	13.26	2.08	30.67	31.5	1.46	0.14
	3	-	-	-	32.8	67.2	-	-
c)	1	-	-	-	27.74	72.26	-	-
	2	7.35	4.5	1.11	37.16	49.88	1.31	0.19
	3	-	-	-	30.05	69.95	-	-

d)	1	-	-	-	10.76	89.24	-	-
	2	16.05	15.69	3.76	45.9	18.6	0.83	0.20
	3	-	-	-	30.30	69.70	-	-
e)	1	-	-	-	28.51	71.49	-	-
	2	12.74	12.47	6.89	43.72	24.18	0.66	0.35
	3	20.52	17.93	1.19	45.58	14.78	1.07	0.10

316

317 ## 4. Conclusions

318 Gold and silver enamels were developed as potential back contacts for CIGS solar cells.
319 The enamels were successfully deposited on ceramic substrates making integrated
320 photovoltaic tiles for the first time. The substrates evidence lack of porosity, mechanical
321 and chemical resistance, and low linear contraction. Different methods of enamel
322 deposition, ink-jet and screen-printing, were applied. The ink-jet proves better
323 effectiveness than screen-printing.

324 Non-vacuum routes for CIGS synthesis (co-precipitation) and deposition (doctor blade)
325 were used. The co-precipitation of selenite precursors results very successful obtaining
326 $CuIn_{0.7}Ga_{0.3}Se_2$ solid solution. Doctor blade technique achieved well-adhered, dense,
327 and homogeneous layers with adequate thickness.

328 Excellent compatibility between CIGS and gold coating was obtained keeping layer
329 width and chemical composition adequate for photovoltaic applications. The band gap
330 measurement confirms the assembly effectiveness.

331 In contrast, silver diffusion leading coating separation was achieved for the silver glaze.
332 The Ag layer results non-ohmic and therefore the back contact unusable.

333

334

335

336

337

Acknowledgements

The authors would like to acknowledge the financial support of the Spanish Ministry of Economy and Competitiveness under the program INNPACTO (IPT-2011-0913-920000). We are also appreciating the characterization assistance of Central Service of Scientific Instrumentation (SCIC) at the University Jaume I and Torrecid Group S.A.

References

[1]M. A. Contreras, M. J. Romero, and R. Noufi, "Characterization of Cu(In,Ga)Se2 materials used in record performance solar cells," *Thin Solid Films*, 511-512 51-54 (2006).

[2]P. Jackson, D. Hariskos, E. Lotter, S. Paetel, R. Wuerz, R. Menner, W. Wischmann, and M. Powalla, "New world record efficiency for Cu(In,Ga)Se2 thin-film solar cells beyond 20%," *Progress in Photovoltaics: Research and Applications*, 19[7] 894-897 (2011).

[3]J. García-Ten, A. Saburit, E. Bernardo, and P. Colombo, "Development of lightweight porcelain stoneware tiles using foaming agents," *Journal of the European Ceramic Society*, 32[4] 745-752 (2012).

[4]J. M. Pérez and M. Romero, "Microstructure and technological properties of porcelain stoneware tiles moulded at different pressures and thicknesses," *Ceramics International*, 40[1] 1365-1377 (2014).

[5]S.-U. Park, R. Sharma, K. Ashok, S. Kang, J.-K. Sim, and C.-R. Lee, "A study on composition, structure and optical properties of copper-poor CIGS thin film deposited by sequential sputtering of CuGa/In and In/(CuGa+In) precursors," *Journal of Crystal Growth*, 359 1-10 (2012).

[6]T. Magorian Friedlmeier, P. Mantilla Pérez, I. Klugius, P. Jackson, O. Kiowski, E. Ahlswede, and M. Powalla, "Optoelectronic characterization of co-evaporated and low-cost Cu(In,Ga)Se2 solar cells, a comparison," *Thin Solid Films*, 535 92-96 (2013).

[7]D. Nam, S. Jung, S. Ahn, J. Gwak, K. Yoon, J. H. Yun, and H. Cheong, "Influence of growth process on optical properties of Cu(In1−xGax)Se2 thin film solar cells," *Thin Solid Films*, 535 118-121 (2013).

[8]ZSW, "New best mark in thin-film solar performance with 21.7 percent efficiency," *Press Release*, 12 1-2 (2014).

[9]D. Lee and K. Yong, "Non-vacuum deposition of CIGS absorber films for low-cost thin film solar cells," *Korean Journal of Chemical Engineering*, 30[7] 1347-1358 (2013).

[10]F. Roux, S. Amtablian, M. Anton, G. Besnard, L. Bilhaut, P. Bommersbach, J. Braillon, C. Cayron, A. Disdier, H. Fournier, J. Garnier, A. Jannaud, J. Jouhannaud, A. Kaminski, N. Karst, S. Noël, S. Perraud, O. Poncelet, O. Raccurt, D. Rapisarda, A. Ricaud, D. Rouchon, M. Roumanie, E. Rouviere, O. Sicardy, F. Sonier, K. Tarasov, F. Tardif, M. Tomassini, and J. Villanova, "Chalcopyrite thin-film solar cells by industry-compatible ink-based process," *Solar Energy Materials and Solar Cells*, 115 86-92 (2013).

[11]T. K. Todorov, O. Gunawan, T. Gokmen, and D. B. Mitzi, "Solution-processed Cu(In,Ga)(S,Se)2absorber yielding a 15.2% efficient solar cell," *Progress in Photovoltaics: Research and Applications*, 21[1] 82-87 (2013).

[12]E. C. T. Todorov, J. F. Sanchez-Royo, J. Carda, and P. Escribano, "CuInS2 Films for Photovoltaic Applications Deposited by a Low-Cost Method," *Chem. Mater.*, 18 3145-3150 (2006).

[13]D. Lee, Y. Choi, and K. Yong, "Morphology and crystal phase evolution of doctor-blade coated CuInSe2 thin films," *Journal of Crystal Growth*, 312[24] 3665-3669 (2010).

[14]F. C. Krebs, "Fabrication and processing of polymer solar cells: A review of printing and coating techniques," *Solar Energy Materials and Solar Cells*, 93[4] 394-412 (2009).

[15]A. R. Uhl, Y. E. Romanyuk, and A. N. Tiwari, "Thin film Cu(In,Ga)Se2 solar cells processed from solution pastes with polymethyl methacrylate binder," *Thin Solid Films*, 519[21] 7259-7263 (2011).

[16]M. Park, S. Ahn, J. H. Yun, J. Gwak, A. Cho, S. Ahn, K. Shin, D. Nam, H. Cheong, and K. Yoon, "Characteristics of Cu(In,Ga)Se2 (CIGS) thin films deposited by a direct solution coating process," *Journal of Alloys and Compounds*, 513 68-74 (2012).

[17]C. P. Liu and C. L. Chuang, "Fabrication of CIGS nanoparticle-ink using ball milling technology for applied in CIGS thin films solar cell," *Powder Technology*, 229 78-83 (2012).

[18]N. G. Dhere, "Scale-up issues of CIGS thin film PV modules," *Solar Energy Materials and Solar Cells*, 95[1] 277-280 (2011).

[19]M. A. Aegerter and M. Mennig, "Sol-Gel Technologies for Glass Producers and Users," Springer, 2004.
[20]I.-S. Park, W. Li, and A. Manthiram, "Fabrication of catalyst-coated membrane-electrode assemblies by doctor blade method and their performance in fuel cells," *Journal of Power Sources*, 195[20] 7078-7082 (2010).
[21]K. Xiong, L. Hou, M. Wu, Y. Huo, W. Mo, Y. Yuan, S. Sun, W. Xu, and E. Wang, "From spin coating to doctor blading: A systematic study on the photovoltaic performance of an isoindigo-based polymer," *Solar Energy Materials and Solar Cells*, 132 252-259 (2015).
[22]K. L. Chopra, P. D. Paulson, and V. Dutta, "Thin-film solar cells: an overview," *Progress in Photovoltaics: Research and Applications*, 12[23] 69-92 (2004).
[23]F. Kessler and D. Rudmann, "Technological aspects of flexible CIGS solar cells and modules," *Solar Energy*, 77[6] 685-695 (2004).
[24]D. Amouzou, P. Guaino, L. Fourdrinier, J.-B. Richir, F. Maseri, and R. Sporken, "Dielectric and diffusion barrier multilayer for Cu(In,Ga)Se2 solar cells integration on stainless steel sheet," *Thin Solid Films*, 542 270-275 (2013).
[25]F. Pianezzi, A. Chirilă, P. Blösch, S. Seyrling, S. Buecheler, L. Kranz, C. Fella, and A. N. Tiwari, "Electronic properties of Cu(In,Ga)Se2solar cells on stainless steel foils without diffusion barrier," *Progress in Photovoltaics: Research and Applications*, 20[3] 253-259 (2012).
[26]K. Moriwaki, M. Nomoto, S. Yuuya, N. Murakami, T. Ohgoh, K. Yamane, S. Ishizuka, and S. Niki, "Monolithically integrated flexible Cu(In,Ga)Se2 solar cells and submodules using newly developed structure metal foil substrate with a dielectric layer," *Solar Energy Materials and Solar Cells*, 112 106-111 (2013).
[27]F. M. G. Gordillo, and C. Calderón, "Electrical and Morphological Properties of Low Resistivity Mo thin Films Prepared by Magnetron Sputtering," *Brazilian Journal of Physics*, 36 982-985 (2005).
[28]A. D. John H. Scofield, D. Albin, B. L. Ballard and P. K. Predecki, "Sputtered Molybdenum Bilayer Back Contact for Copper Indium Diselenide-Based polycrystalline Thin-Film Solar Cell," *Thin Solid Films*, 260[1] 26-31 (1994).
[29]L. Assmann, J. C. Bernède, A. Drici, C. Amory, E. Halgand, and M. Morsli, "Study of the Mo thin films and Mo/CIGS interface properties," *Applied Surface Science*, 246[1-3] 159-166 (2005).
[30]P. T. Erslev, J. Lee, G. M. Hanket, W. N. Shafarman, and J. D. Cohen, "The electronic structure of Cu(In1-xGax)Se2 alloyed with silver," *Thin Solid Films*, 519[21] 7296-7299 (2011).
[31]R. J. Matson, O. Jamjoum, A. D. Buonaquisti, P. E. Russell, L. L. Kazmerski, P. Sheldon, and R. K. Ahrenkiel, "Metal contacts to CuInSe2," *Solar Cells*, 11[3] 301-305 (1984).
[32]A. Romeo, M. Terheggen, D. Abou-Ras, D. L. Bätzner, F. J. Haug, M. Kälin, D. Rudmann, and A. N. Tiwari, "Development of thin-film Cu(In,Ga)Se2 and CdTe solar cells," *Progress in Photovoltaics: Research and Applications*, 12[23] 93-111 (2004).
[33]K. Orgassa, H. W. Schock, and J. H. Werner, "Alternative back contact materials for thin film Cu(In,Ga)Se2 solar cells," *Thin Solid Films*, 431-432 387-391 (2003).
[34]P. Blösch, S. Nishiwaki, T. Jaeger, L. Kranz, F. Pianezzi, A. Chirilă, P. Reinhard, S. Buecheler, and A. N. Tiwari, "Alternative back contact designs for Cu(In,Ga)Se2 solar cells on polyimide foils," *Thin Solid Films*, 535 220-223 (2013).
[35]P. Blösch, D. Güttler, A. Chirila, and A. N. Tiwari, "Optimization of Ti/TiN/Mo back contact properties for Cu(In,Ga)Se2 solar cells on polyimide foils," *Thin Solid Films*, 519[21] 7453-7457 (2011).
[36]P. M. P. Salomé, V. Fjallstrom, A. Hultqvist, P. Szaniawski, U. Zimmermann, and M. Edoff, "The effect of Mo back contact ageing on Cu(In,Ga)Se2thin-film solar cells," *Progress in Photovoltaics: Research and Applications*, 22[1] 83-89 (2014).

445 [37]S. M. Kong, R. Fan, S. H. Jung, and C. W. Chung, "Characterization of Cu(In,Ga)Se2 thin films
446 prepared by RF magnetron sputtering using a single target without selenization,"
447 *Journal of Industrial and Engineering Chemistry*, 19[4] 1320-1324 (2013).
448 [38]S. Pak and J. Kim, "Structural analysis of Cu(In,Ga)Se2 films fabricated by using sputtering and
449 post-selenization," *Current Applied Physics*, 13[6] 1046-1049 (2013).
450 [39]W. Thongkham, A. Pankiew, K. Yoodee, and S. Chatraphorn, "Enhancing efficiency of
451 Cu(In,Ga)Se2 solar cells on flexible stainless steel foils using NaF co-evaporation," *Solar*
452 *Energy*, 92 189-195 (2013).
453 [40]U. Z. J. Lindahl, P. Szaniawski, T. Torndahl, A. Hultqvist, P. Salome, C. Platzer-Bjorkman, and
454 M. Edoff, "Inline Cu(In,Ga)Se2 Co-evaporation for High-Efficiency Solar Cells and
455 Modules," *Journal of Photovoltaics*, 3[3] 1100-1105 (2013).
456 [41]J. A. Hollingsworth, K. K. Banger, M. H. C. Jin, J. D. Harris, J. E. Cowen, E. W. Bohannan, J. A.
457 Switzer, W. E. Buhro, and A. F. Hepp, "Single source precursors for fabrication of I–III–
458 VI2 thin-film solar cells via spray CVD," *Thin Solid Films*, 431-432 63-67 (2003).
459 [42]S. Jung, S. Ahn, J. H. Yun, J. Gwak, D. Kim, and K. Yoon, "Effects of Ga contents on properties
460 of CIGS thin films and solar cells fabricated by co-evaporation technique," *Current*
461 *Applied Physics*, 10[4] 990-996 (2010).
462 [43]A. L. Patterson, "The Scherrer Formula for X-Ray Particle Size Determination," *Physical*
463 *Review*, 56,[10] 978-982 (1939).
464 [44]M. A. Contreras, L. M. Mansfield, B. Egaas, J. Li, M. Romero, R. Noufi, E. Rudiger-Voigt, and
465 W. Mannstadt, "Wide bandgap Cu(In,Ga)Se2solar cells with improved energy
466 conversion efficiency," *Progress in Photovoltaics: Research and Applications*, 20[7]
467 843-850 (2012).

468

469

470

471